

## Effect of Capillary Water on Electrochemical Corrosion Behaviour and Mechanism of X70 Steel in Silty Clay

Jianjian Wei<sup>1</sup>, Bin He<sup>1,\*</sup>, Yongxiang Feng<sup>1</sup>, Junlong Xu<sup>1</sup>, Dengqin Liang<sup>1</sup>, Lifeng Hou<sup>2</sup>, Pengju Han<sup>1</sup>, Xiaohong Bai<sup>1</sup>

<sup>1</sup> College of Civil Engineering, Taiyuan University of Technology, Taiyuan, 030024, China

<sup>2</sup> College of Materials Science and Engineering, Taiyuan University of Technology, Taiyuan, 030024, China

\*E-mail: [hebin@tyut.edu.cn](mailto:hebin@tyut.edu.cn)

Received: 17 July 2022 / Accepted: 16 August 2022 / Published: 10 September 2022

---

In this paper, we simulated a corrosive environment with dynamically changing capillary water wetting fronts in silty clay by indoor simulation tests and studied the electrochemical corrosion behaviour of X70 steel in the corrosive environment with rising capillary water at different ages by electrochemical means. The results show that the electrochemical corrosion behaviour of X70 steel in silty clay is significantly influenced by changes in the capillary water wetting front. The equivalent circuit model for the electrochemical corrosion of X70 steel is a dynamic process that changes with the position of the capillary water wetting front. The polarization resistance  $R_p$  of X70 steel at position 1# of the soil column shows a pattern of decreasing and then increasing with increasing burial time, while the polarization resistance  $R_p$  of X70 steel at position 2# of the soil column shows a pattern that roughly increases gradually with increasing burial time. The polarization resistance  $R_p$  of X70 steel at the position of the capillary water wetting front decreases significantly, the cathodic branch of the polarization curve shifts significantly to the right, and the corrosion rate increases dramatically. At the same time, the ions in the soil with the rise of capillary water to the upper part of the soil column will also lead to a significant reduction of the upper X70 steel polarization resistance  $R_p$  and a sharp increase of the corrosion rate. In addition, the presence of clay particles has a catalytic effect on the cathodic reaction of X70 steel, an effect that is more pronounced when the X70 steel is in the TPB region.

---

**Keywords:** Electrochemical impedance spectroscopy (EIS); polarization curve; polarization resistance; capillary water wetting front

### 1. INTRODUCTION

With the rapid development of urbanisation and the construction of the energy industry in China, the country has promoted the large-scale construction of long-distance buried pipelines for the transport

of oil and gas to improve the energy mix and to ensure the safe supply of oil and gas to all regions. An increasing number of pipeline steels are being used, with X70 and X80 steels being used as the main pipeline steels for this type of construction [1-3]. The corrosion of transport oil and gas pipelines is mainly due to redox reactions between the media in the soil environment and the pipeline steel, thus accelerating the corrosion of steel materials, which places higher demands on the safety and durability of oil and gas pipelines [4-6]. In recent years, a large number of domestic and foreign scholars have carried out in-depth research on the corrosion of buried metals [7-10]. Wang et al. [11] used finite element simulation analysis, dynamic potential polarization curves, electrochemical impedance spectroscopy, scanning electron microscopy and three-dimensional ultradepth microscopy to comprehensively investigate general and localised corrosion under a combination of tensile stress and erosion. The results show that both tensile stress and erosion can independently contribute to general corrosion. Wang et al. [12] investigated the corrosion behaviour of X70 pipeline steel under three different corrosion conditions. The results showed that with increasing AC density, the open circuit potential of X70 steel samples showed a negative shift and an increase in the corrosion rate under the three different corrosion conditions. The corrosion rate of X70 steel increased significantly when 30 A/m DC interference was applied. Zhu et al. [13] used the weak polarization curve method and electrochemical impedance spectroscopy to investigate the effects of  $\text{Cl}^-$  and direct stray currents on the soil corrosion of three grounded grid materials. The results showed that both factors,  $\text{Cl}^-$  and direct stray current, could accelerate the corrosion rate of the earthing grid materials. The magnitude of the DC stray current density affects the type of mass transfer and response frequency of the anodic and cathodic reactions of the earthing materials, while the  $\text{Cl}^-$  content of the soil only affects the mass transfer rate of the electrode materials in the electrochemical impedance spectrogram. In addition, many scholars have also focused on the influence of water content and changes in the solid-liquid-gas phase on corrosion during the corrosion of buried metals [14-16]. Robert et al. [17] exposed mild steel specimens to fine-graded clay soils with different moisture contents and different levels of compaction for different times. The results of the study obtained showed that the maximum soil moisture loss and corrosion pit depth were achieved at 17-18% soil moisture content for all exposure and compaction levels. Yang et al. [18] developed array electrode test plates for the study of the corrosion behaviour in NaCl solutions and wet soil environments to investigate macroscopic galvanic coupling corrosion of carbon steel near the gas-liquid interface. The test results show that the coexistence of macro- and microcell corrosion changes the location of maximum corrosion and infer a relationship between the actual current density and the microhole current density. The results of these studies have contributed to the development and improvement of metal corrosion theory. However, there is no current research on the corrosion process of metals in a corrosive environment with dynamically changing solid-liquid-gas phases in unsaturated soils. This study simulates the electrochemical corrosion behaviour of X70 steel during the dynamic change of the wetting front position under the capillary water rise in engineering reality through indoor simulation tests. This is important for us to better understand the corrosion characteristics of X70 steel during the dynamic corrosion process of capillary water rise and the improvement of metal corrosion theory.

## 2. MATERIALS AND EXPERIMENTS

### 2.1. Test material preparation

The test soil was taken from a site in Taiyuan, Shanxi Province, China. The soil was naturally dried and sieved through a 2 mm sieve. The particle size distribution of the soil is shown in Figure 1. The basic physicochemical soil property parameters are shown in Table 1. Deionized water was mixed with spare soil with sufficient agitation to obtain NaCl-free uncontaminated soil. After dissolving a certain amount of NaCl (analytical grade) in deionized water, the NaCl solution was mixed with alternate soil with sufficient agitation to obtain a saline soil with a NaCl content of 1.0%. The mass moisture content of both soil samples was kept consistent, which were left to stand in a constant temperature and humidity chamber for 24 h.

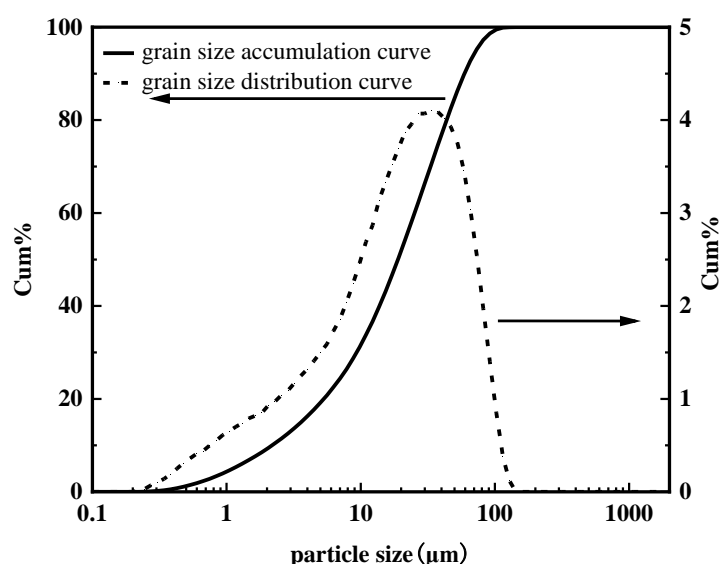


**Figure 1.** Soil particle size distribution

**Table 1.** Basic physical and chemical properties of the soil

Parameters	Natural water content (%)	Liquid limit (%)	Plastic limit (%)	Plastic index	pH
Values	12.24	30.30	18.80	11.50	7.2

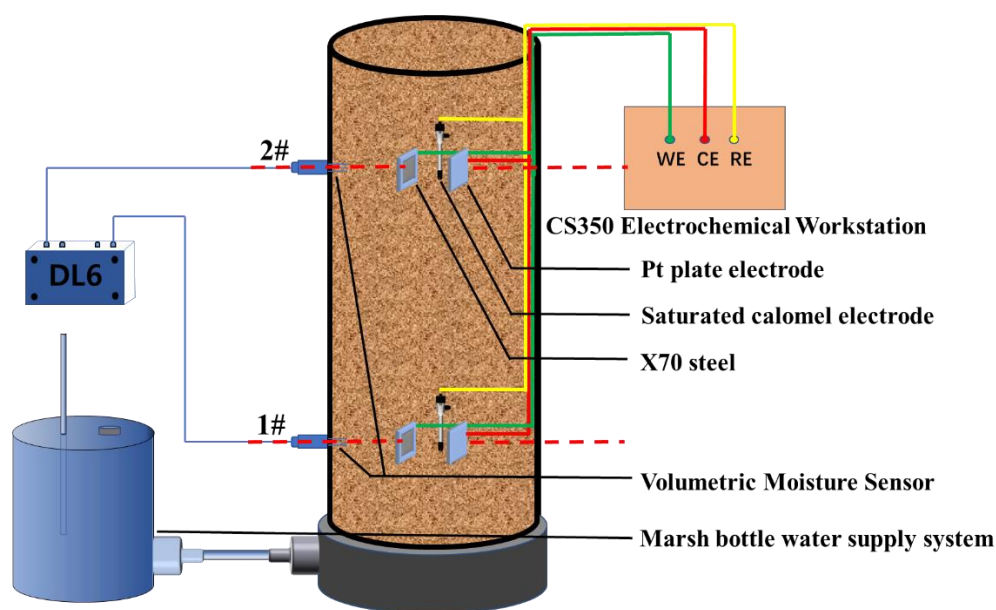
The main chemical composition parameters of the X70 steel used in this test are listed in Table 2. The X70 steel sample size in this test was 15 mm × 15 mm × 2 mm. The X70 steel samples were processed on a grinding machine with 800-2000 grit sandpaper grade by grade, polished one by one and finally ultrasonically cleaned in deionized water. For the electrochemical measurements, copper conductors were soldered to the X70 steel, leaving a 10 mm × 10 mm working surface on the surface of the X70 steel, and the remaining surface was covered with epoxy resin.

**Table 2.** Main chemical composition of X70 pipeline steel (wt.%)

C	Si	Mn	P	Cr	Ni	Mo	Cu	Co	V	S	Fe
0.0645	0.201	1.906	0.0119	0.021	0.021	0.234	0.012	0.013	0.011	<0.0005	Balance

## 2.2. Test procedure

A Geo-experts 1D soil column apparatus was used to simulate soil erosion in unsaturated soils with capillary rise. As shown in Figure 2, the Geo-experts 1D soil column instrument consists of a constant water supply system, a Plexiglas cylinder, an ML2x moisture sensor and a DL6 monitoring and storage device. The ML2x moisture sensors were positioned 120 mm and 570 mm from the bottom of the soil column, and the two positions were named positions 1# and 2#, respectively.

**Figure 2.** Schematic diagram of the experimental installation

First, before burying the X70 steel sheet inside the glass cylinder, the Plexiglas cylinder was fixed to the test base, and a lubricant was evenly applied to the inside wall to make the inside of the Plexiglas cylinder smooth. Next, a filter paper was laid on the bottom of the Plexiglas drum, and the prepared moist standard sand was laid on top of the filter paper and compacted to a thickness of 1 cm. This allowed the capillary water to rise evenly. Finally, the test soil, prepared in advance with a certain moisture content, was compacted in layers to ensure that the density was the same throughout the column. During the compaction of the test soil in layers, a certain mass of test soil was weighed and compacted to a certain height each time. Continued compaction of the soil to position 1# of the soil column placed the X70 steel sheet and the electrodes required for the test in the soil in the relative positions shown in Figure 3. The soil was compacted in layers to position 2#, and the X70 steel sheet and the electrodes required for the test were placed in the same way.

For this test, a CS350 electrochemical workstation was used. A three-electrode system was used for the electrochemical tests, X70 steel was used as the working electrode (WE), a platinum electrode was used as the counter electrode (CE) and a saturated calomel electrode was used as the reference electrode (RE). Before the electrochemical test, the CS350 instrument was switched on for 30 minutes to allow the potential to stabilise. EIS was conducted over a frequency range of  $10^{-1} \sim 10^5$  Hz with a logarithmic sweep and an applied sine wave AC amplitude of 10 mV. The polarization curve was obtained over a sweep range of -0.75 to 3 V with a sweep frequency of 2 mV/s.

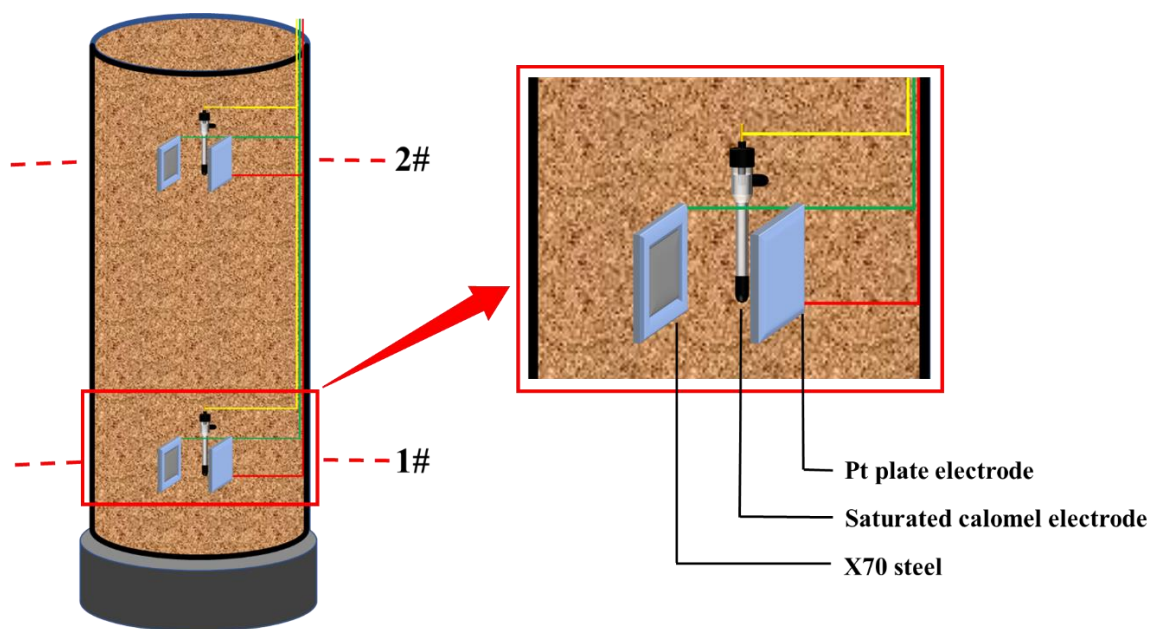
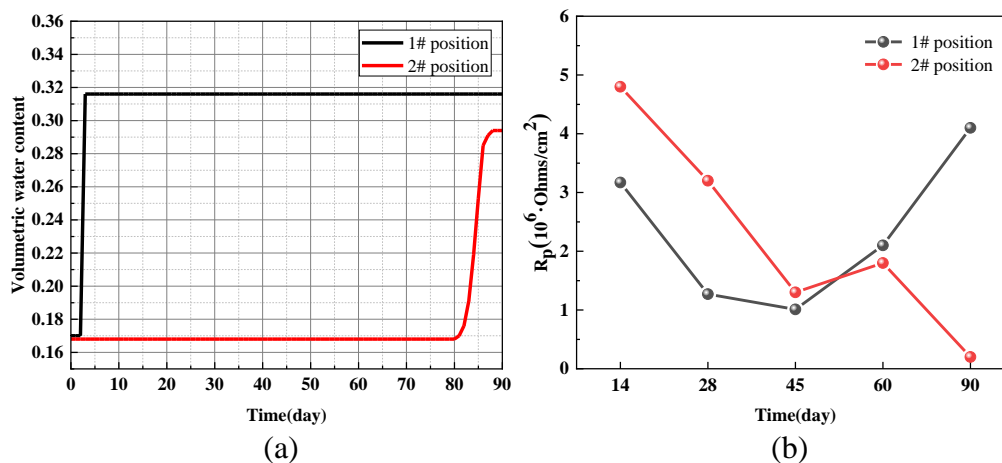
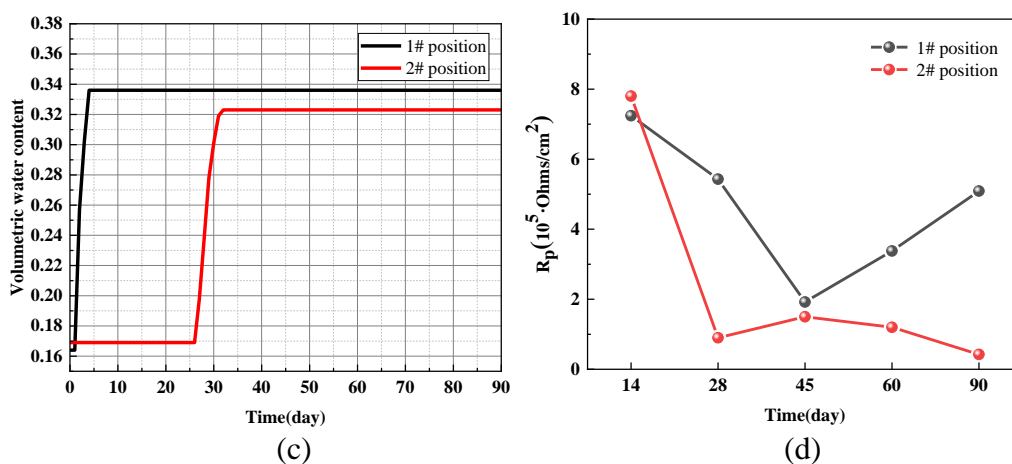


Figure 3. Diagram of the relative positions of the electrodes

### 3. RESULTS AND ANALYSIS

#### 3.1. Variation of the polarization resistance $R_p$ with the age of corrosion



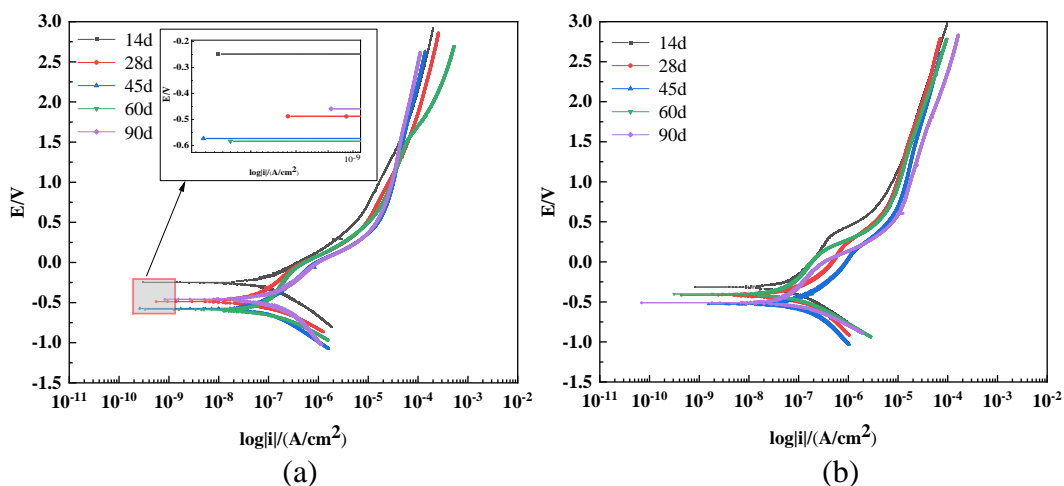


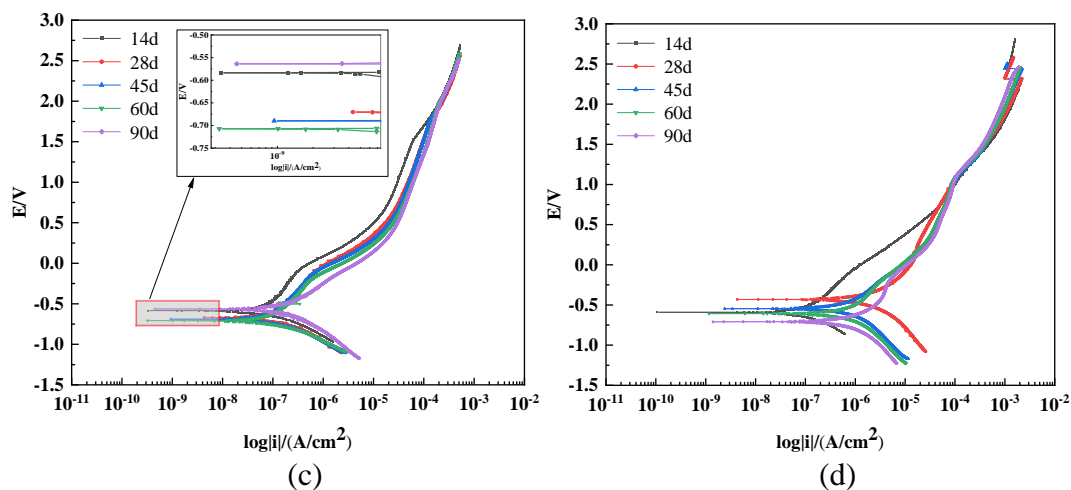
**Figure 4.** Curves of the volumetric water content and polarization resistance of the X70 steel surface at different locations in the soil column as a function of time: (a) Curves of the volumetric water content of soil columns with 0.0% NaCl as a function of time; (b) curves of the polarization resistance of X70 steel with 0.0% NaCl in earth columns as a function of time; (c) curves of the volumetric water content of soil columns with 1.0% NaCl as a function of time; and (d) curves of the polarization resistance of X70 steel with 1.0% NaCl in earth columns as a function of time.

Figure 4 shows the variation in the volumetric water content and the polarization resistance ( $R_p$ ) of the X70 steel with burial time at locations 1# and 2# of the soil column. As shown in Figure 4, the polarization resistance  $R_p$  of X70 steel at height position 1# in a corrosive soil environment with 0.0% and 1.0% NaCl shows a trend of first decreasing and then increasing with increasing burial time. In addition, the results of Choi and Kim's study showed that the polarization resistance is inversely proportional to the corrosion rate of metal [19]. This means that the corrosion rate of X70 steel at height position 1# in a corrosive soil environment with 0.0% and 1.0% NaCl shows a pattern of increasing and then decreasing with increasing burial time. The reason for this pattern may be that the formation of a protective layer of dense corrosion products starting in the later stages of corrosion (45 days) hinders ion and charge exchange and eventually leads to a tendency for the polarization resistance to increase. In addition, the high water content of location 1# for a long period of time makes it easier for the clay particles to play a "gluing" role [20], which makes the corrosion products more tightly bound to the clay particles and contributes to the increase in polarization resistance. As seen in Figure 4, the polarization resistance  $R_p$  at location 2# for two different NaCl content soil corrosion environments shows an overall decreasing trend with increasing corrosion age. The corrosion rate of X70 steel at location 2# roughly shows an increasing trend with increasing corrosion age. The cause of this phenomenon can be attributed to the change in the physicochemical properties of the corrosive environment of X70 steel due to the rise of capillary water. As seen in Figure 4, the polarization resistance of X70 steel at position 2# in a 0.0% NaCl corrosive soil environment decreases sharply at 90 days. Similarly, the polarization resistance of X70 steel at position 2# in a 1.0% NaCl corrosive soil environment also decreases sharply at 28 days. The reason for this phenomenon can be found in the curves for the change in the volumetric water content at location 2# in Figure 4 for two different NaCl content soil corrosion environments. The rise in capillary water in a corrosive soil environment with 0.0% NaCl content placed the capillary water wetting front near position 2# at 90 days, which caused a sharp rise in the volumetric water content at this position. In

addition, Barranco et al. showed that the soil dielectric constant increases with increasing volumetric water content in the soil and that the increase in the soil dielectric constant leads to a decrease in the polarization resistance [20]. At the same time, because of the presence of the capillary water wetting front near position 2#, making the X70 steel interface at this time in the solid/liquid/gas three-phase interface zone (TPB) [16, 21], the cathodic process increased significantly, and the corrosion rate increased sharply. Similarly, the large drop in the polarization resistance at position 2# at 28 days in a corrosive soil environment with a NaCl content of 1.0% is due to the same reason. In addition, the polarization resistance at position 2# in the soil corrosion environment with a NaCl content of 1.0% also showed a law of decreasing with increasing age after 45 days. This can be attributed to the accumulation of NaCl ions in the corrosive environment caused by the rise of capillary water to position 2# of the soil column, which increases the soil dielectric constant and reduces the polarization resistance at this position. Figure 4 shows that the volumetric water content at position 2# in the soil corrosion environment with a NaCl content of 1.0% changed sharply at 28 days, which was caused by the rise in the capillary water wetting front at this position. The reason why the polarization resistance at ages between 28 days and 45 days did not show a regular decrease with age is the hysteresis of the migration of salt relative to the migration of water in the corrosive soil environment [22]. It is not difficult to find that the polarization resistance in a corrosive soil environment with a NaCl content of 1.0% is an order of magnitude smaller than that in a corrosive soil environment without salt because the dielectric constant of saline soil is much larger than that of non-saline soil, which is why metal corrosion is more severe in saline soils[23].

### 3.2. Measurement of polarization curves





**Figure 5.** Variation of X70 steel polarization curves in soil columns with time: (a) polarization curve of X70 steel at position 1# in a soil column with 0.0% NaCl; (b) polarization curve of X70 steel at position 2# in a soil column with 0.0% NaCl; (c) polarization curve of X70 steel at position 1# in a soil column with 1.0% NaCl; and (d) polarization curve of X70 steel at position 2# in a soil column with 1.0% NaCl.

The polarization curves for X70 steel are shown in Figure 5. The polarization parameters for X70 steel were obtained by Tafel fitting of the polarization curves using CView2 fitting software and are listed in Table 3. Figure 5 shows that the self-corrosion potential of X70 steel at positions 1# and 2# in the soil corrosion environment with a NaCl content of 1.0% is slightly negative compared with that in the soil corrosion environment with a NaCl content of 0.0%, which implies that in the soil corrosion environment with a NaCl content of 1.0%, the corrosion thermodynamic trend of X70 steel in the soil corrosion environment with a NaCl content of 1.0% is larger, and X70 steel is more prone to corrosion. At the same time, the self-corrosion potential of X70 steel at position 1# in the two different NaCl soil corrosion environments in Figure 5 shows a pattern of decreasing and then increasing with increasing corrosion time. This indicates that as corrosion proceeds, the thermodynamic trend of the corrosion of X70 steel at this location first increases and then decreases. The reason why the self-corrosion potential of X70 steel increases in the late stages of corrosion is that the thermodynamic trend of corrosion decreases because the  $Fe^{2+}$  generated by the dissolution of X70 steel does not diffuse easily into the X70 steel surface pore solution. This can be attributed to the hindering effect of the corrosion product layer of X70 steel at position 1# [24]. It is easy to see that at 28 days of corrosion age, the cathodic branch of the polarization curve is at the far right compared to the other ages. The reason for this can be attributed to the fact that at 28 days at position 2#, X70 steel is in the vicinity of the capillary water wetting front, i.e., the solid/liquid/gas three-phase interface (TPB). In addition, the polarization curve of X70 steel at 45 days and after the age of corrosion at position 2# of the 1.0% NaCl soil column showed a significant shift to the right, which was also attributed to the rise of capillary water. The presence of NaCl in the corrosive environment of the soil, with the rise of capillary water in the soil pore space, leads to aggregation towards position 2#, and the presence of NaCl promotes the ion exchange capacity at the electrode interface, thus accelerating the corrosion of X70 steel and shifting the polarization curve to the right.

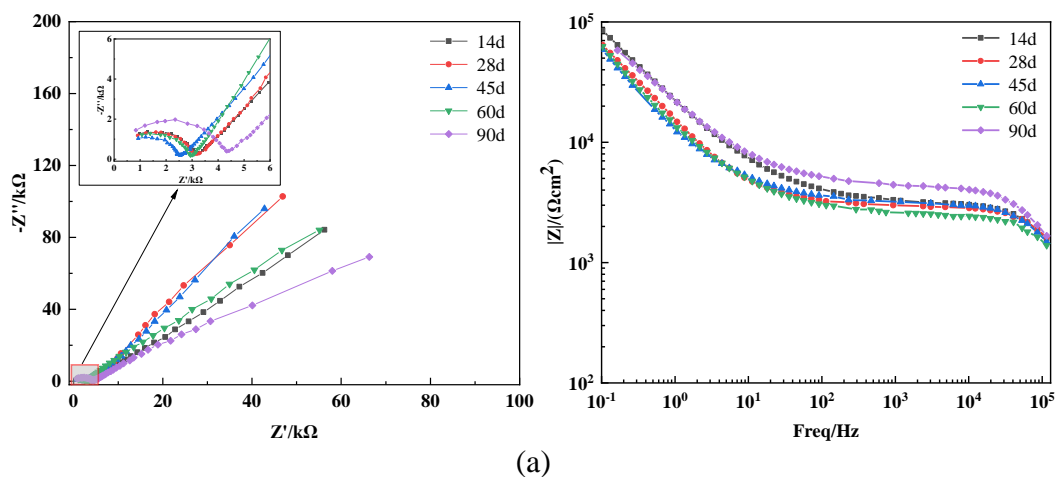
**Table 3.** Polarization parameters of X70 steel

NaCl Content	Position	Time (days)	$R_p$ ( $\Omega/\text{cm}^2$ )	$I_{\text{corr}}$ ( $\text{A}/\text{cm}^2$ )	$E_{\text{corr}}$ (V)	Corrosion Rate (mm/a)
0.0%	1#	14	$3.17 \times 10^6$	$2.41 \times 10^{-8}$	-0.249	$3.12 \times 10^{-4}$
		28	$1.27 \times 10^6$	$3.58 \times 10^{-8}$	-0.482	$4.63 \times 10^{-4}$
		45	$1.01 \times 10^6$	$10.10 \times 10^{-8}$	-0.571	$13.1 \times 10^{-4}$
		60	$2.10 \times 10^6$	$3.16 \times 10^{-8}$	-0.588	$4.58 \times 10^{-4}$
		90	$4.10 \times 10^6$	$3.04 \times 10^{-8}$	-0.458	$4.10 \times 10^{-4}$
	2#	14	$4.80 \times 10^6$	$1.27 \times 10^{-8}$	-0.312	$1.49 \times 10^{-4}$
		28	$3.20 \times 10^6$	$2.92 \times 10^{-8}$	-0.406	$3.43 \times 10^{-4}$
		45	$1.30 \times 10^6$	$15.9 \times 10^{-8}$	-0.531	$18.76 \times 10^{-4}$
		60	$1.80 \times 10^6$	$8.23 \times 10^{-8}$	-0.386	$9.23 \times 10^{-4}$
		90	$0.20 \times 10^6$	$17.9 \times 10^{-8}$	-0.509	$21.12 \times 10^{-4}$
1.0%	1#	14	$7.24 \times 10^5$	$4.07 \times 10^{-8}$	-0.582	$7.13 \times 10^{-4}$
		28	$5.43 \times 10^5$	$6.08 \times 10^{-8}$	-0.674	$7.16 \times 10^{-4}$
		45	$1.92 \times 10^5$	$16.20 \times 10^{-8}$	-0.683	$20.39 \times 10^{-4}$
		60	$3.38 \times 10^5$	$10.13 \times 10^{-8}$	-0.709	$13.45 \times 10^{-4}$
		90	$5.09 \times 10^5$	$9.28 \times 10^{-8}$	-0.564	$10.48 \times 10^{-4}$
	2#	14	$7.80 \times 10^5$	$0.39 \times 10^{-7}$	-0.601	$0.64 \times 10^{-3}$
		28	$0.90 \times 10^5$	$9.92 \times 10^{-7}$	-0.396	$18.36 \times 10^{-3}$
		45	$1.50 \times 10^5$	$5.31 \times 10^{-7}$	-0.552	$5.93 \times 10^{-3}$
		60	$1.20 \times 10^5$	$8.81 \times 10^{-7}$	-0.621	$15.33 \times 10^{-3}$
		90	$0.43 \times 10^5$	$14.60 \times 10^{-7}$	-0.718	$30.05 \times 10^{-3}$

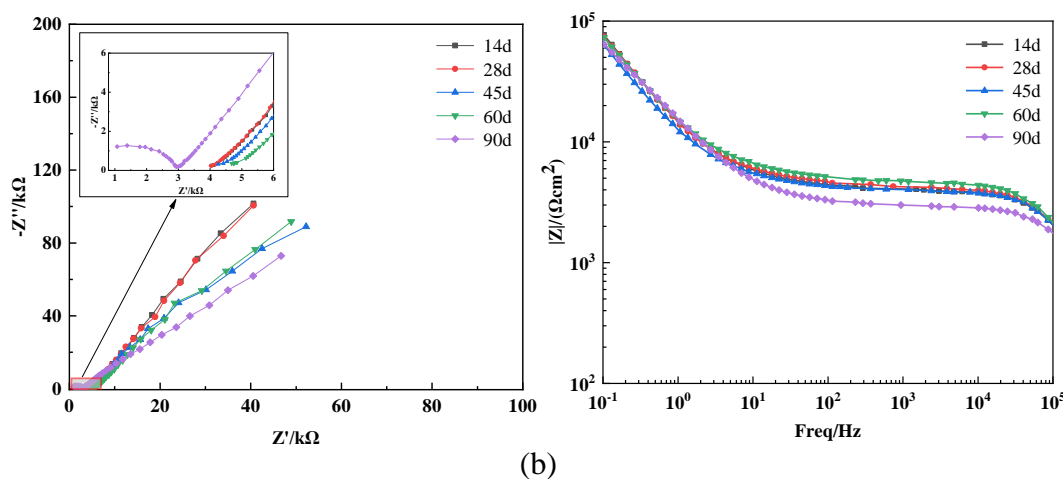
Figure 5 shows that the polarization curve of X70 steel in a corrosive soil environment with a NaCl content of 1.0% is shifted in the positive direction of the axes compared to a corrosive soil environment without NaCl. This is because the presence of NaCl in the corrosive soil environment promotes the corrosion of X70 steel [25]. We can clearly see in Table 3 that the corrosion current density and corrosion rate of X70 in a corrosive soil environment with a NaCl content of 1.0% are higher than those in a corrosive soil environment with a NaCl content of 0.0%. We believe that the cause of this phenomenon is primarily the addition of  $\text{Cl}^-$  to the soil environment in the traditional sense of promoting the anodic dissolution of metals [26]. In addition, the physicochemical properties of the soil in a corrosive environment can also influence the corrosion of metals in that environment. The soil used in this experiment is a powdery clayey soil, and the presence of a large number of fine clayey soil particles

is a characteristic of this soil. The  $Al^{3+}$  in the clay lattice is often partially replaced by  $Mg^{2+}$  and  $Ca^{2+}$  in the soil, thus making the clay lattice negatively charged. To maintain electrical neutrality, the clay surface inevitably adsorbs some positive ions, which in turn leave the surface due to hydration and form a double electric layer. The thickness of the electric double layer of monovalent  $Na^+$  is twice that of divalent  $Mg^{2+}$  and  $Ca^{2+}$ ; therefore, when there is a large amount of  $Na^+$  in the corrosive environment, the thickness of the double layer between the soil particles increases, the repulsive force is greater than the suction force, the net potential energy is expressed as a repulsive force, and the soil sample is more dispersed [27]. In the capillary water wetting front position, when the degree of soil dispersion increases, the degree of droplet dispersion in the corrosive environment increases, the TPB area on the surface of X70 steel increases, and the cathodic corrosion reaction is intensified. This situation in the capillary water wetting front position of X70 steel corrosion is particularly obvious, greatly accelerating the X70 steel cathodic corrosion reaction. In this test, the specific performance is observed with the NaCl content of 1.0% in the soil corrosion environment at 28 days, where the capillary water wetting front rose to position 2# of the soil column. At this time, the cathodic branch of the polarization curve exhibited a substantial shift to the right. This eventually manifested itself as a sharp increase in the corrosion current density and corrosion rate for X70 steel at this location.

### 3.3. Electrochemical impedance spectroscopy



(a)



(b)

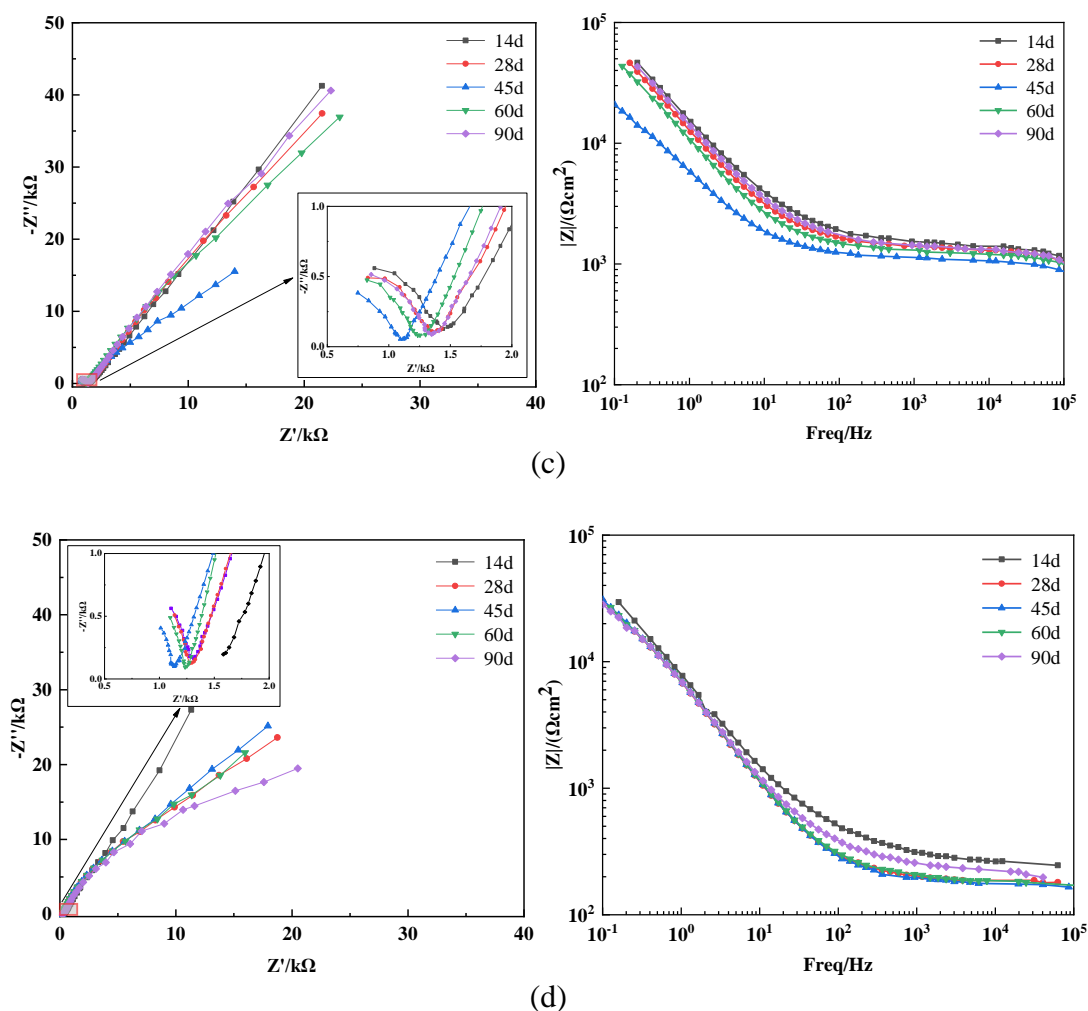


**Figure 6.** Nyquist plots and Bode plots of X70 steel: (a) position 1# in a column of soil with 0.0% NaCl content; (b) position 2# in a column of soil with 0.0% NaCl content; (c) position 1# in a column of soil with 1.0% NaCl content; and (d) position 2# in a column of soil with 1.0% NaCl content.

As seen from Figure 6, the Nyquist diagram for X70 steel consists of one or two impedance arcs and shows a diffusion process through the porous layer in the low frequency region [28]. From Figure 6, we can see that the Nyquist plot for the X70 steel at position 1# in the soil column for both 0.0% and 1.0% NaCl consists of two capacitive resistance arcs, which indicates that there are two time parameters in the equivalent circuit model for the X70 steel at that position. However, the Nyquist diagram for X70 steel at position 2# consists of either one capacitive arc or two capacitive arcs. The reason for this difference in the Nyquist diagram for X70 steel can be attributed to the change in the corrosive environment of X70 steel due to the rise in capillary water. The X70 steel at position 2# of the soil column with 0.0% NaCl content has only two capacitive arcs of resistance at 90 days in the Nyquist plot, and the other four ages have only one capacitive arc of resistance. This is because the X70 steel at position 2# is above the capillary water wetting front until 90 days of age. The Nyquist diagram for X70 steel at position 2# in a 1.0% NaCl soil column consists of two capacitive arcs of resistance for all ages except 14 days. This is due to the position of the X70 steel in the capillary water wetting front or below the wetting front within 28 days and beyond. Clay particles tend to act more readily as "glues" in capillary water wetting fronts and environments below the wetting fronts. This allows the corrosion

products on the surface of X70 steel to bind more closely to the clay particles. At this point the clay particles attached to the X70 steel-soil interface have an impact on the corrosion reaction of X70 steel. This directly leads to differences in the equivalent circuit model.

The electrochemical equivalent circuit model for X70 steel in powdered clay subjected to capillary water rise is shown in Figure 7. Figure 7(a) shows the equivalent circuit model for X70 steel at the capillary water wetting front and below the capillary water wetting front. Figure 7(b) shows the equivalent circuit model for X70 steel at a position above the capillary water wetting front.

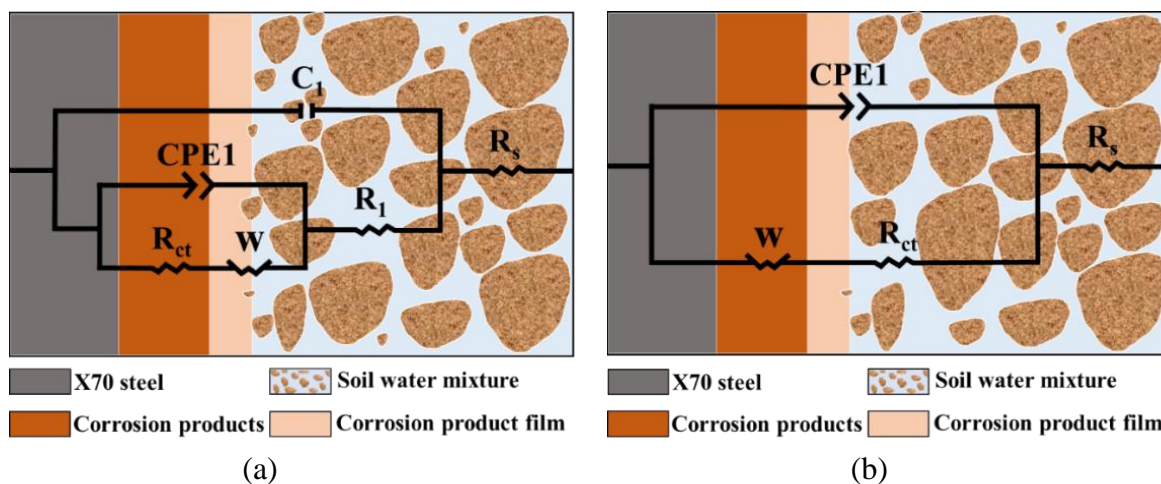


**Figure 7.** Equivalent circuit model for X70 steel: (a) Capillary water wetting front and position below the wetting front and (b) capillary water wetting above the front.

The correlation fitting parameters for X70 steel at locations 1# and 2# in the soil columns with 0.0% and 1.0% NaCl contents obtained by ZView2 software are listed in Table 4, where  $R_s$  represents the soil resistance,  $R_1$  represents the transfer resistance of the clay particles to the pore solution,  $C_1$  represents the clay bilayer capacitance,  $R_{ct}$  represents the charge transfer resistance,  $W$  represents the Weber impedance Warburg, and the constant phase angle element CPE1 represents the corrosion product bilayer capacitance. As seen from Table 4, the soil resistance  $R_s$  at position 1# in both the 0 and 1.0% NaCl content soil corrosion systems showed a gradual increase with time. The reason for this phenomenon is that the soil column at position 1# was below the wetting front of the capillary water for the period from 14 to 90 days. Ions in the soil at position 1# gathered higher in the column as the capillary water rose, which caused the ion concentration at position 1# to decrease. This resulted in the soil resistance  $R_s$  at location 1# exhibiting a pattern of increasing resistance with time. The soil resistance  $R_s$  at position 2# in the soil with 0.0% NaCl decreased significantly at 90 days. This is because at 90 days, the capillary water rises to position 2# in the soil column, causing a sharp increase in the water content at this position. In addition, Table 4 shows that the soil resistance  $R_s$  at position 2# in the soil column with a NaCl content of 1.0% decreased after 45 days. This is because the ions in the soil column accumulate at position 2# of the column as the capillary water rises, and the increase in ion concentration causes the soil resistance  $R_s$  to decrease at this position.

**Table 4.** Equivalent circuit parameters for X70 steel

NaCl content	Position	Time (days)	$R_s$ ( $\Omega/\text{cm}^2$ )	$R_1$ ( $\Omega/\text{cm}^2$ )	$C_1$ ( $\text{F}/\text{cm}^2$ )	$R_{ct}$ ( $\Omega/\text{cm}^2$ )	W1 -R	W1 -T	W1 -P	CPE -T	CPE -P
0.0%	1#	14	332.60	1450.40	$8.14 \times 10^{-7}$	68400.00	$5.68 \times 10^6$	8.49	0.60	$6.66 \times 10^{-9}$	0.65
		28	329.50	946.20	$5.48 \times 10^{-7}$	31100.00	$2.19 \times 10^6$	1.25	0.71	$6.66 \times 10^{-9}$	0.81
		45	394.20	3122.10	$6.66 \times 10^{-7}$	11460.00	$8.49 \times 10^6$	0.15	0.69	$6.66 \times 10^{-9}$	0.75
		60	415.90	988.62	$9.56 \times 10^{-7}$	40500.00	$9.08 \times 10^5$	21.18	0.80	$6.66 \times 10^{-9}$	0.66
		90	456.80	768.60	$9.01 \times 10^{-7}$	61520.00	$1.60 \times 10^6$	9.84	0.76	$6.66 \times 10^{-9}$	0.57
	2#	14	465.10	—	—	71200.00	$6.61 \times 10^6$	1.58	0.62	$6.66 \times 10^{-9}$	0.66
		28	491.30	—	—	33580.00	$5.38 \times 10^6$	8.65	0.59	$6.66 \times 10^{-9}$	0.62
		45	502.50	—	—	8620.00	$6.21 \times 10^6$	1.25	0.68	$6.66 \times 10^{-9}$	0.52
		60	486.10	—	—	13640.00	$1.02 \times 10^6$	3.33	0.73	$6.66 \times 10^{-9}$	0.76
		90	351.00	1886.40	$8.14 \times 10^{-7}$	6580.00	$3.69 \times 10^6$	14.58	0.79	$6.66 \times 10^{-9}$	0.78
1.0%	1#	14	251.10	1162.30	$6.65 \times 10^{-9}$	51900.00	$2.11 \times 10^5$	31.08	0.83	$6.66 \times 10^{-9}$	0.63
		28	268.50	786.60	$9.10 \times 10^{-9}$	28800.00	$6.82 \times 10^6$	9.90	0.81	$6.66 \times 10^{-9}$	0.69
		45	260.30	1056.20	$7.15 \times 10^{-9}$	8310.00	$6.60 \times 10^5$	17.15	0.72	$6.66 \times 10^{-9}$	0.79
		60	301.00	886.80	$5.69 \times 10^{-9}$	12540.00	$5.08 \times 10^6$	6.30	0.66	$6.66 \times 10^{-9}$	0.73
		90	388.70	847.10	$8.13 \times 10^{-9}$	13500.00	$9.98 \times 10^6$	1.29	0.86	$6.66 \times 10^{-9}$	0.71
	2#	14	351.80	—	—	9110.00	$7.19 \times 10^5$	7.74	0.61	$6.66 \times 10^{-9}$	0.75
		28	311.10	914.80	$8.68 \times 10^{-9}$	2860.00	$1.68 \times 10^6$	4.59	0.82	$6.66 \times 10^{-9}$	0.65
		45	158.00	1042.50	$6.25 \times 10^{-9}$	5920.00	$8.15 \times 10^6$	16.33	0.60	$6.66 \times 10^{-9}$	0.81
		60	134.80	660.40	$3.34 \times 10^{-9}$	3040.00	$3.60 \times 10^5$	0.88	0.78	$6.66 \times 10^{-9}$	0.75
		90	112.20	365.10	$1.05 \times 10^{-9}$	843.00	$6.08 \times 10^6$	4.55	0.80	$6.66 \times 10^{-9}$	0.61

Table 4 shows that the transfer resistance  $R_1$  between clay particles and pore solution in the soil column with a NaCl content of 1.0% is generally smaller than that in the column without NaCl. This indicates that there is a relationship between the transfer resistance  $R_1$  of the clay particles to the pore solution and the ion concentration in the soil. From Table 4, we can see that the clay bilayer capacitance  $C_1$  at position 2# in the soil column with a NaCl content of 1.0% exhibits a decreasing trend with increasing time. The reason for the decrease in the capacitance  $C_1$  of the clay bilayer may be the increase in the thickness of the bilayer [29]. Studies have shown that the charge transfer resistance  $R_{ct}$  is inversely

proportional to the corrosion rate of the metal. As seen from Table 4, the charge transfer resistance  $R_{ct}$  at position 1# in the soil column with 0.0% and 1.0% NaCl content both show a pattern of decreasing and then increasing with time. This indicates that the corrosion rate of X70 steel shows a pattern of increasing and then decreasing with time, which is consistent with the conclusions drawn from the polarization resistance and polarization curve fitting parameters. In addition, it can be seen from Table 4 that the charge transfer resistance  $R_{ct}$  of X70 steel at the wetting front position will decrease sharply. This is because the increase in water at the interface between the electrode and the soil increases the conductivity of the conductive path [30].

### 3.4. Microscopic morphology and corrosion mechanism analysis

The microscopic images of the corrosion products on the surface of X70 steel at 90 days and the 3D contours of the corrosion pits on the surface of X70 steel after removal of the corrosion products are shown in Figure 8. The 3D profile of the corrosion pits in Figure 8 is scanned from the deepest part of the corrosion pits on the X70 steel substrate. The position 0.00 in the scale in the upper left corner of the image is the deepest corrosion pit on the X70 steel surface. The maximum value of the scale represents the distance of the deepest corrosion pit from the uncorroded part of the metal substrate, i.e., the depth of the deepest corrosion pit on the metal surface. It can be seen from the figure that the corrosion of X70 steel belongs to local corrosion, and the surface of X70 steel is accompanied by local corrosion pits [31].

As shown in the surface microscopic image of X70 steel in Figure 8, all surfaces of X70 steel are covered with corrosion products, and there is a clear delamination of the corrosion product coverings [32]. This is due to the anodic dissolution of metals or the formation of metal oxides as well as hydrated metal oxides during the anodic reaction of metals in the corrosion reaction. Deposits of dissolved metal ions and oxides as well as hydroxides occur at different times, which results in a clear layering of the corrosion products of the metal. At the same time, because the corrosion environment is soil porous medium, the corrosion products on the surface of X70 steel are discontinuous [33]. The corrosion product film on the surface of X70 steel is often accompanied by pore and crack defects through which the reducing medium in the soil corrosion system reaches the X70 steel matrix to promote further corrosion of the metal [34]. In addition, aggressive ions from the soil can also enter the inner layer through the loose and porous corrosion product layer, allowing the reaction to continue. As a result, the film of corrosion products on the metal surface is often ineffective in preventing the metal from continuing to corrode. As shown in Figure 8, the corrosion products of X70 steel include diamond-shaped flake corrosion products, petal-shaped corrosion products, needle-shaped corrosion products, etc. It is clear from the microscopic images in Figure 8 that the amount of corrosion products covering the surface of X70 steel in the soil column with a NaCl content of 1.0% is significantly greater than that in the soil column without NaCl and the corrosion products are thicker and fluffier.

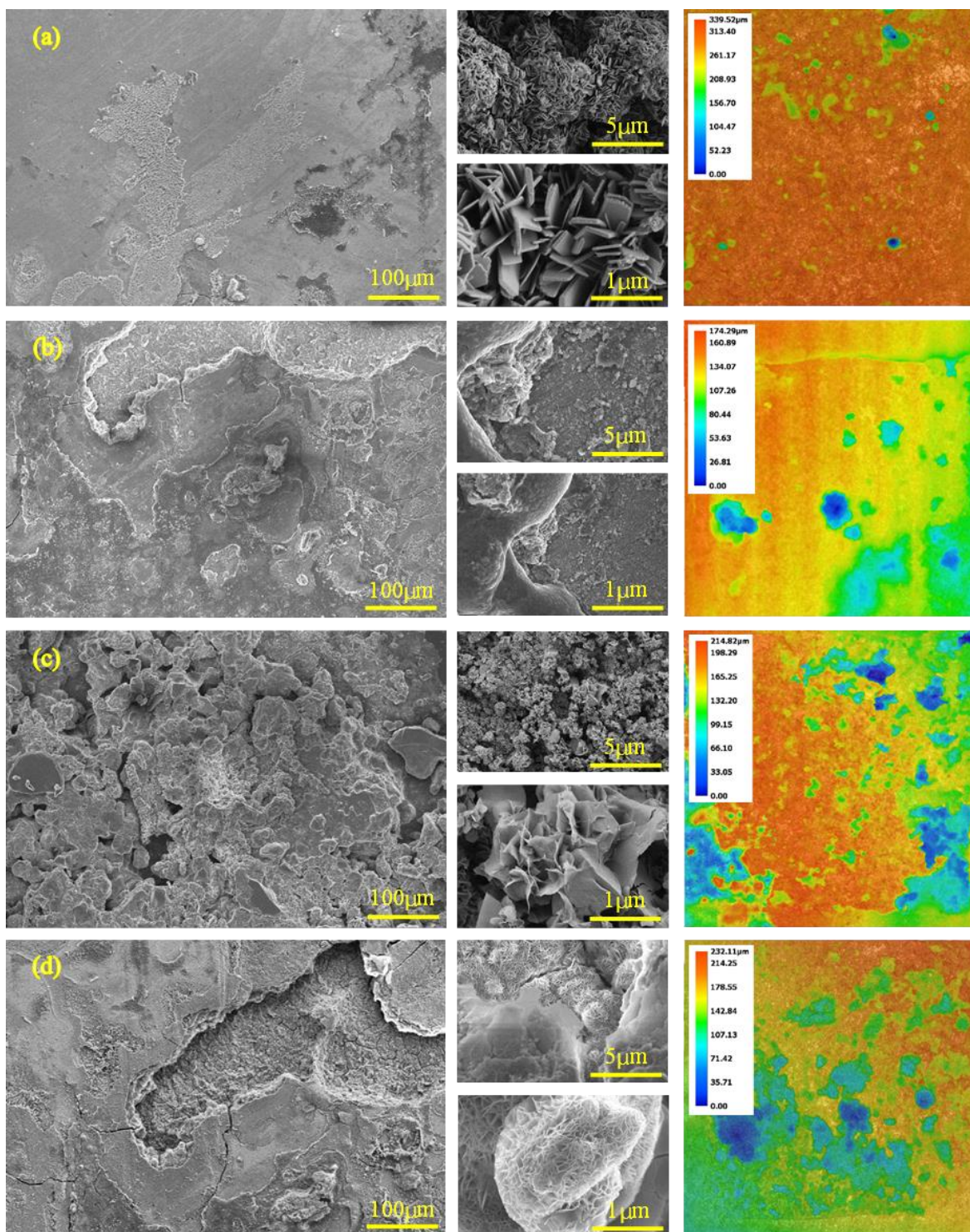


**Figure 8.** Microscopic images of the corrosion products on the surface of X70 steel at 90 days and schematic 3D contours of the corrosion pits on the surface of X70 steel after removal of the corrosion products: (a) Position 1# of the soil column with 0.0% NaCl content; (b) position 2# of the soil column with 0.0% NaCl content; (c) position 1# of the soil column with 1.0% NaCl content; and (d) position 2# of the soil column with 1.0% NaCl content.

This indicates that the corrosion rate of X70 steel is greater in the 1.0% NaCl soil column. This is consistent with the prevailing view that the presence of aggressive Cl<sup>-</sup> promotes the occurrence of

electrochemical corrosion of the metal. In addition, the same conclusion can be drawn from the 3D profile of the corrosion pits on the surface of X70 steel in Figure 8.

The number of corrosion pits and the area of collapse on the surface of X70 steel in the soil column with a NaCl content of 1.0% are significantly larger than those in the soil column without NaCl. In addition, it is not difficult to find that in the same soil column, the corrosion of X70 steel is often more severe at position 2#. One of the reasons for this is that the ions in the soil column are concentrated at position 2# with the migration of capillary water. Another reason would be the difference in the morphology of the solid-liquid-gas phase between positions 1# and 2# of the same soil column due to the rise of the capillary water. Soil, as a very complex corrosive environment, includes three phases, solid, liquid and gas, and changes in the solid-liquid-gas phase can have a significant impact on the corrosion of X70 steel [35]. Due to the rise of capillary water, location 1# is permanently below the wetting front of capillary water, and although the higher water content makes charge transfer easier [36], the lack of oxygen in the corrosive environment inhibits metal corrosion. The X70 steel at position 2# in the soil column is first above the capillary water wetting front for a certain period of time. Then, as the capillary water rises, the X70 steel is placed in the capillary water wetting front position; at this time, the X70 steel is located in the solid-liquid-gas three-phase border (TPB) region, which suddenly increases the corrosion rate of X70 steel [16]. This is because the rate of the cathodic reaction (Equation 1) in the TPB region is greatly enhanced. In contrast, the test soil used in this experiment is a silty clay, and the hydroxyl groups (SiOH) that may be exposed on the surface and edges of the clay particles adsorbed on the metal surfaces decompose into  $\text{SiO}^-$  and  $\text{H}^+$  (Equation 2). The  $\text{H}^+$  consumes some of the  $\text{OH}^-$  generated by the cathodic reaction (Equation 3), which causes the cathodic reaction to accelerate further. A schematic diagram of the mechanism of action is shown in Figure 9. The increase in the metal cathodic reaction rate due to the TPB region is more pronounced when NaCl is present in the corrosive environment. The reason for this is that the thickness of the clay double layer is greater when NaCl is present in the soil and the clay particles are more dispersed.

This results in a greater number of TPB zones and a more pronounced acceleration of the cathodic response to metal corrosion. Finally, because of the rise of capillary water, position 2# of the soil column is also in the capillary water wetting front position below; at this time, the corrosion environment tends to saturate. The presence of clay particles at locations below the capillary water wetting front makes diffusion of oxygen very difficult, and thus oxygen is not a major reducing agent in saturated pulverised clays. At this point, the hydroxyl iron oxide ( $\text{FeOOH}$ ) in the corrosion product acts as a cathodic depolarising agent replacing the reducing agent role of oxygen and dominating the cathodic reaction of corrosion (Equation 4). Iron oxide is reduced by participating in depolarization, i.e., an autocatalytic process is formed during the corrosion of the metal[28].

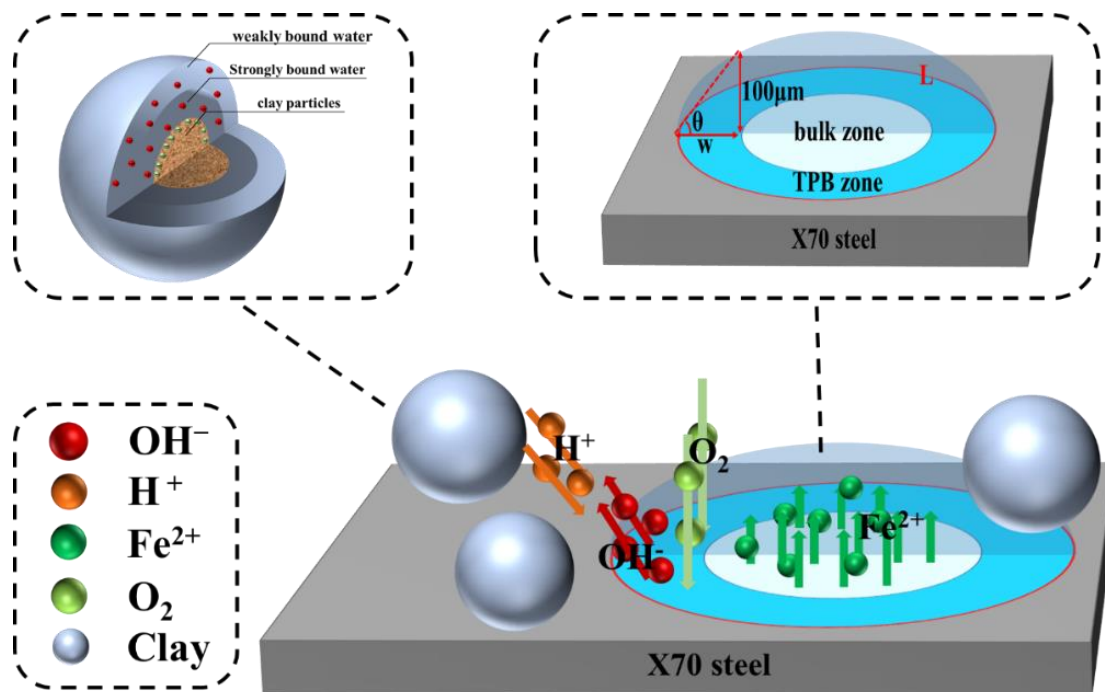
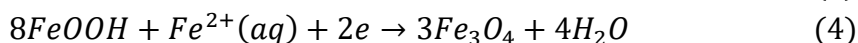
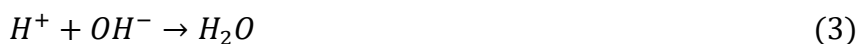


**Figure 9.** Schematic diagram of the mechanism of the soil-steel interface in a silty clay loam



#### 4. CONCLUSIONS

In this paper, the capillary action in saline soils was simulated by a Geo-experts 1D soil column instrument, and the electrochemical corrosion behaviour of X70 steel at different ages in a corrosive environment with rising capillary water was investigated by electrochemical means. The conclusions are as follows:

(1) The results of the polarisation resistance  $R_p$  analysis show that the polarisation resistance  $R_p$  of X70 steel at location 1# of the soil column shows a pattern of decreasing and then increasing with increasing burial time, while the polarisation resistance  $R_p$  of X70 steel at location 2# of the soil column shows a roughly gradual increase with increasing burial time. In addition, the polarisation resistance  $R_p$  of the X70 steel at position 2# of the soil column decreases significantly due to a sharp increase in the volumetric water content at the location of the capillary water wetting front, and the polarisation resistance  $R_p$  also decreases due to salt build-up at this location.

(2) The results of the polarisation curve analysis show that the corrosion current density and corrosion rate of X70 steel in the corrosive environment of a soil with a NaCl content of 1.0% are significantly higher than those of a soil without NaCl. The self-corrosion potential of X70 steel at position 1# of the soil column decreases and then increases with increasing corrosion time, and the

thermodynamic trend of corrosion increases and then decreases. When the NaCl content of the soil column is 1.0%, for X70 steel at position 2# in the capillary water wetting front position, the cathodic branch of the polarization curve exhibited a significant right shift, and the cathodic corrosion rate increased significantly.

(3) The results of the electrochemical impedance analysis show that the equivalent circuit model for the electrochemical corrosion of X70 steel is significantly influenced by the rise of capillary water. The equivalent circuit model for the electrochemical corrosion of X70 steel is a dynamic process that changes with the position of the capillary water wetting front. The soil resistance  $R_s$  increases in the corrosion regime at position 1# due to the ions rising higher up the soil column with the capillary water, while at position 2# the soil resistance  $R_s$  decreases significantly due to the presence of wetting fronts and the accumulation of ions.

(4) The microscopic images show that the surface of X70 steel is covered with significantly more corrosion products in the soil column with 1.0% NaCl than in the soil column without NaCl. The soil column with 1.0% NaCl has a thicker layer of X70 steel corrosion products, a larger number of corrosion pits in the metal matrix and a larger ulcerated area. In addition, the presence of clay particles has a catalytic effect on the cathodic reaction of X70 steel, an effect that is more pronounced when the X70 steel is in the TPB region.

#### ACKNOWLEDGEMENTS

This work was funded by National Natural Science Foundation of China (Grant No. 41807256, 51178287), Applied Basic Research Program in Shanxi Province (Grant No. 20210302123139).

#### References

1. A. V. Pogozhev, Y. I. Matrosov, M. B. Klyukvin, M. Y. Matrosov, and G. N. Konovalov, *Metallurgist*, 57(2013)66.
2. Z. Wang, Z. Zhou, W. Xu, L. Yang, B. Zhang and Y. Li, *Eng. Failure Anal.*, 115(2020)104659.
3. F. Xie, Z. Wang, D. Wang and S. Yin, *Appl.Phys.A*, 126(2020)868.
4. N. I. I. Mansor, S. Abdullah, A. K. Ariffin and J. Syarif, *Eng. Failure Anal.*, 42(2014)353.
5. S. K. Sharma and S. Maheshwari, *J. Nat. Gas Sci. Eng.*, 38(2017)203.
6. B. Liu, C. Du, X. Li, D. Wang, J. Xu, C. Sun, L. Yang and B. Hou, *J. Mater. Eng. Perform.*, 31(2021)1769.
7. Y. Huang, D. Xu, L. Y. Huang, Y. T. Lou, J. B. Muhadesi, H. C. Qian, E. Z. Zhou, B. J. Wang, X. T. Li, Z. Jiang, S. J. Liu, D. W. Zhang and C. Y. Jiang, *npj Biofilms Microbiomes*, 7(2021).
8. S. Suganya, R. Jeyalakshmi and N. P. Rajamane, *Mater. Today: Proc.*, 5(2018)8735.
9. Y. Fu, J. Kou and C. Du, *Anti-Corros. Methods Mater.*, 66(2019)868.
10. Y. Wang, X. Zuo and J. Li, *Steel Res. Int.*, 86(2015)1260.
11. W. Wang, J. Hu, X. Yuan, L. Zhou, J. Yu, Z. Zhang and X. Zhong, *Constr. Build. Mater.*, 342(2022)127972.
12. X. Wang, Z. Wang, Y. Chen, X. Song and C. Xu, *J. Mater. Eng. Perform.*, 28(2019)1958.
13. Z. Zhu, C. Shi, Y. Zhang and Z. Liu, *Anti-Corros. Methods Mater.*, 67(2020)73.
14. R. Hendi, H. Saifi, K. Belmokre, M. Ouadah, B. Smili and B. Talhi, *Mater. Res. Express*, 5(2018)36523.
15. Q. Zhang, S. L. Larson, J. H. Ballard, P. Cheah, X. Zhu, H. M. Knotek-Smith and F. X. Han, *MethodsX*, 7(2020).

16. J. Jiang, J. Wang, Y. H. Lu and J. Z. Hu, *Electrochim. Acta*, 54(2009)1426.
17. R. B. Petersen and R. E. Melchers, *Corros. Eng., Sci. Technol.*, 54(2019)587.
18. M. Yang and S. Kainuma, *Corros. Eng., Sci. Technol.*, 56(2021)690.
19. Y. S. Choi and J. G. Kim, *Corrosion*, 56(2000)1202.
20. V. Barranco, J. Carpentier and G. Grundmeier, *Electrochim. Acta*, 49(2004)1999.
21. J. Wang, L. Liang and J. Jiang, *Electrochem. Commun.*, 10(2008)1788.
22. J. Wei, B. He, Y. Feng, L. Hou, P. Han and X. Bai, *Mater.*, 15(2022) 3426.
23. J. Liu, P. Yang and Z. Yang, *Cold Reg. Sci. Technol.*, 178(2020)103127.
24. F. Sun, R. Xie, B. He, Z. Chen, X. Bai and P. Han, *Int. J. Electrochem. Sci.*, 16(2021)150878.
25. Z. X. Yang, B. Kan, J. X. Li, Y. J. Su and L. J. Qiao, *J. Electroanal. Chem.*, 822(2018)123.
26. F. Xue, X. Wei, J. Dong, C. Wang and W. Ke, *J. Mater. Sci. Technol.*, 35(2019)596.
27. H. C. S. Filho, R. B. Saldanha, C. G. Rocha and N. C. Consoli, *J. Mater. Civ. Eng.*, 33(2021).
28. M. Yan, C. Sun, J. Xu, J. Dong and W. Ke, *Corros. Sci.*, 80(2014)309.
29. M. Özcan, İ. Dehri and M. Erbil, *Appl. Surf. Sci.*, 236(2004)155.
30. X. Liu, P. Han, F. Ma, B. He, X. Wang, F. Sun, Z. Chen and X. Bai, *Int. J. Electrochem. Sci.*, 17(2022) 220844.
31. G. Qi, X. Qin, J. Xie, P. Han and B. He, *RSC Adv*, 12(2022) 20929.
32. X. Yu, B. Gong, Q. Gao, Y. Zhao, C. Tian and J. Zhang, *Appl. Therm. Eng.*, 127(2017)1164.
33. B. He, C. Lu, P. Han and X. Bai, *Eng. Fail. Anal.*, 59(2016).
34. H. Ma, B. Zhao, Z. Liu, C. Du and B. Shou, *Constr. Build. Mater.*, 243(2020)118203.
35. R. Hirata, A. Ooi, E. Tada and A. Nishikata, *Corros. Sci.*, 189(2021)109568.
36. L. Quej-Aké, N. Nava, M. A. Espinosa-Medina, H. B. Liu, J. L. Alamilla and E. Sosa, *Corros. Eng., Sci. Technol.*, 50(2014)311.